CLM - R 136

CLM - R 136

UKAEA RESEARCH GROUP

Report

NEUTRONICS OF CELLULAR BLANKETS FOR FUSION REACTORS

G CONSTANTINE
J J BENGSTON
H H SAMUELSON

CULHAM LABORATORY
Abingdon Oxfordshire
1975

Available from H. M. Stationery Office

C 18

£1.00

UDC
621.039.634:539.125.5

CLM-R 136
FTSG(74)P53

NEUTRONICS OF CELLULAR BLANKETS FOR FUSION REACTORS

by

G. CONSTANTINE†
J.J. BENGSTON†
H.H. SAMUELSON*

ABSTRACT

Early models of a fusion reactor blanket based on a toroidal first wall backed by liquid lithium can be quickly discounted because of the impossibility of maintenance and repair. A more practical engineering solution has been proposed in which the blanket comprises replaceable cylindrical cells in a close nested array. This paper examines the neutronic consequences in terms of increased neutron leakage from the blanket and breeding losses due to the cusp shaped gaps between these cells.

Culham Laboratory
Abingdon, Oxon, OX14 3DB, UK
(Euratom-UKAEA Fusion Association)

† at AERE, Harwell, Oxon
* on leave from Connecticut State University, Connecticut, USA

SBN: 85311 033 6

SECTION PAGE

CONTENTS

Glossary of Terms

ρ	torus minor radius
R	torus major radius
R/ρ	aspect ratio
ω	angular co-ordinate of point on the toroid surface measured around the minor circumference from the point closest to the major axis
y and r	cell radius
a	plasma minor radius
h	cell depth, i.e. blanket thickness
α	diam/pitch ratio of blanket cells at outer end
β	diam/pitch ratio of blanket cells at first wall end

1. INTRODUCTION

A considerable amount of physics effort has been devoted to the neutronics problems of the toroidal fusion reactor blanket/magnet shield system, including consideration of tritium breeding, activation, transmutation, neutron damage, heat deposition rates etc. Generally speaking the calculations have been performed on idealised systems in which the vacuum containment is in the form of a continuous wall around the plasma, behind which lie in turn, layers of breeding materials (with structural materials mixed in homogeneously), reflector, magnet shielding, magnets etc. This is the well-known "onion skin" model.

The geometrical problems associated with the toroidal shape of the blanket are usually ignored, the torus being "opened out" into an infinite cylinder. This approximation neglects neutron flux variations around the minor circumference of the torus. Some estimates, however, have been made of this effect as a function of torus aspect ratio[1].

Recent work at Culham[2] has shown that there are very real engineering objections to the "onion skin" model. Because of the inevitability of periodic replacement of parts of the first wall and structure during the reactor life and the need to achieve this with minimum outage time, a modular system is being developed in which the blanket comprises a large number of cylindrical cells filled with breeding material packed around a toroidal volume containing the plasma. The cells can be replaced a few at a time at scheduled shutdowns or in the event of untimely failure. This is described fully by George et al[3]. A hexagonal shape was originally considered for the cells on the basis that this would represent a minimal departure from the "onion skin" model of the blanket. In a blanket which uses liquid lithium for both breeding and heat transfer, high pressures are generated in the flowing lithium by magnetic forces and a hexagonal cell would raise prohibitive stressing problems[4]. To allow the hexagonal cells to touch would be (a) unsatisfactory because of the possibility of diffusion bonding, but in any case (b) impossible because of the simultaneous restrictions of toroidal geometry and the need to be able to extract the cells. This paper examines some consequences of departing further from the "onion skin" model by using cylindrical cells for a toroidal fusion reactor blanket.

A preliminary calculation (see Appendix A) showed that the neutron transmission through the cusp-shaped region between three adjacent cylinders (Fig 1) is typically less than 1% for the primary

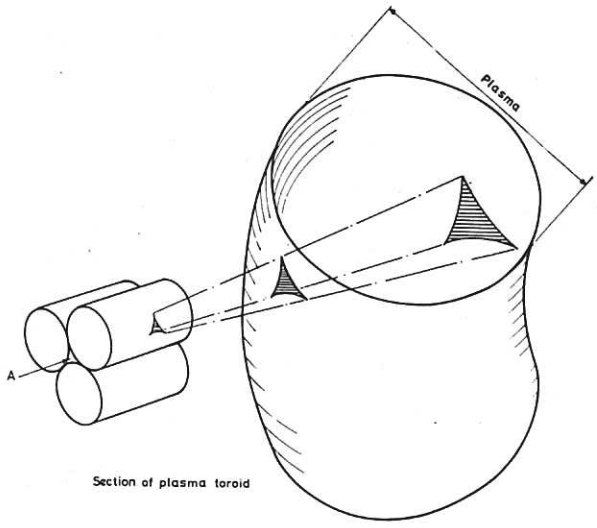

Fig.1 Line of sight between adjacent blanket cells.

14 MeV neutrons from the plasma and only slightly more for neutrons backscattered from the opposite wall. However this does not take into account the effects of the gap on neutrons other than those which penetrate the full thickness of the blanket while remaining in the gap. Recent work at Harwell has therefore been directed at accounting for these in a comprehensive manner, using the Monte Carlo code SPECIFIC II[5] described in Appendix B.

To be consistent with fusion reactor studies at Culham and Harwell, typical values have been taken for the dimensions of the torus. These are major radius 17.8 m, and minor radius 6 m, with a plasma radius of 4.8 m. These dimensions are not sacrosanct, representing only those current at the time this study was started.

2. NEUTRONICS MODELLING OF AN INHOMOGENEOUS BLANKET

As remarked above neutronics calculations on fusion reactor blankets have most frequently been carried out on an infinite cylindrical model to represent the torus "opened out". While this gives a fairly adequate representation of an "onion skin" model, in which the plasma, blanket, reflector and magnet shield are regarded as consecutive layers, when the blanket is formed of cells arranged end-on around the torus the problem cannot be tackled by the geometry routines of the SPECIFIC code; however, with appropriate approximations neutron motion through the blanket can be satisfactorily represented by modelling only a portion of it, complete with cylindrical cells and the gaps between them. The angular distribution of the 14 MeV neutron current

incident on the first wall ends of the cells must be adequately simulated, as must the condition that the lower energy neutrons reflected back into the plasma space will return to the blanket.

SPECIFIC can deal with a nest of concentric cylinders and has facilities for including off-axis cylinders which, however, must be parallel to the Z-axis of the problem space. A hexagonal array of cylindrical cells can be set up easily by specifying their depths, radii and (x , y) coordinates of their axes. The 14 MeV neutron source distribution is represented by a source distributed throughout a large cylindrical space below the cell array as shown in Fig 2. As shown in Appendix C, when

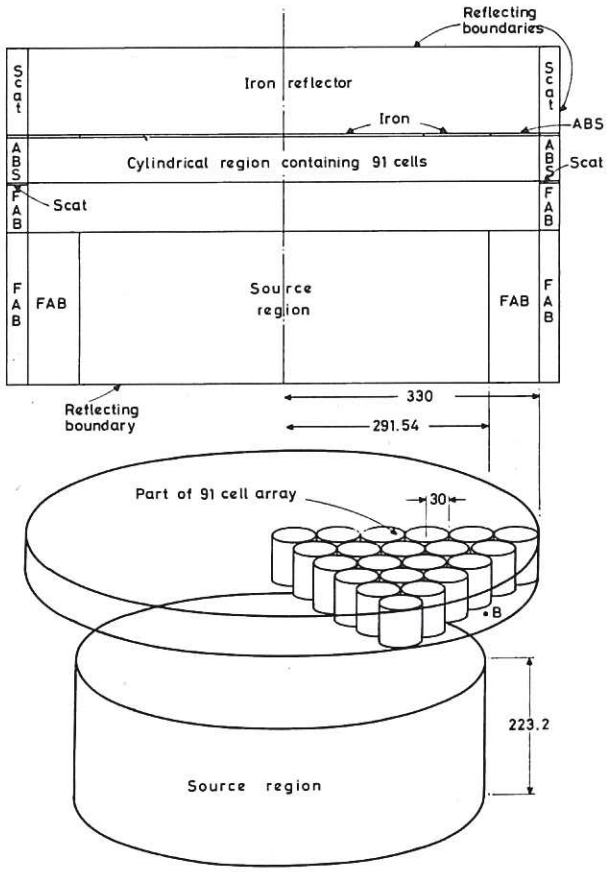

Fig.2 Problem arrangement for SPECIFIC calculations.

the dimensions of the cylinder are suitably chosen, this gives a close approximation to the angular distribution of neutrons arriving at the first wall from a toroidal plasma.

The condition that the currents of lower energy neutrons leaving and entering the first wall must be equal (since the plasma neither produces or absorbs them) has to be satisfied. To ensure this use must be made of a SPECIFIC facility for reflecting neutrons at the problem boundaries. Appendix D details the steps necessary to achieve this while leaving unaffected the angular distribution of 14 MeV neutrons arriving at the first wall. Fig 2 shows the model of the source, multi-cell array and reflector used for the SPECIFIC calculations.

3. TOROID GEOMETRY PROBLEMS

Within its limitations of parallel cylinders the SPECIFIC model must be corrected to simulate the array of cells in a toroidal reactor blanket. There are several consequences of the fact that the cells are located on a curved surface.

(a) Since the gaps between them are tapered the mean density of the blanket is reduced further than is the case with close-packed parallel cells. The reduction in density depends on the two components of the surface curvature, and is discussed in Appendix E.

(b) There are paths through an array of cells along which neutrons can stream unimpeded from the first wall to the reflector end of the blanket. The probability of a neutron so doing depends on the geometry of the gaps between the cells. This is evaluated in Appendix F, in terms of the cell diameter to pitch ratios at the rear wall and first wall, α and β respectively. The resulting visibility parameter VIS is proportional to the neutron current passing through the gaps between cells at the rear of the blanket for a given isotropic flux incident at the first wall end. The variation of VIS with α and β is shown for parallel gaps ($\alpha = \beta$) and tapered gaps with the cells touching at the first wall end ($\beta = 1$) in Fig 3. Leakage through tapered gaps can be simulated by using the parallel cell SPECIFIC model with a cell diameter/pitch ratio offering the same value of VIS.

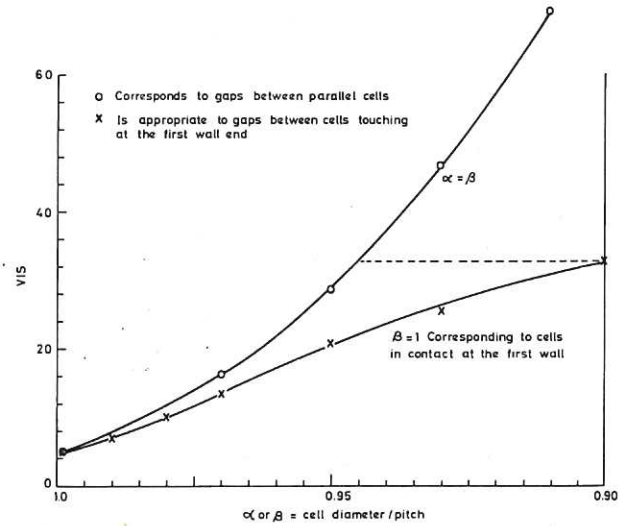

Fig.3 Visibility (VIS) through inter cellular gaps.

(c) Since the cells are arranged on a curved surface it is not possible to close-pack them in a hexagonal lattice. Two immediate possibilities can be envisaged: (i) the cells may vary in radius according to their position around the torus minor circumference, as illustrated in Fig 4, or

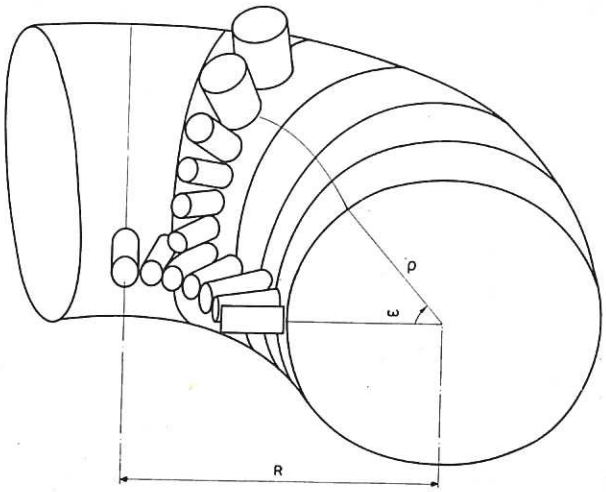

Fig.4 Cylindrical cells fitted around a torus.

(ii) they may be arranged in hexagonal arrays on a relatively few plane surfaces which fit together in a "lobster back" configuration to make up the toroidal blanket structure. In the latter case the present SPECIFIC model would give an excellent representation of all but the regions of intersection between adjacent planes of cells.

4. CALCULATIONS WITH SPECIFIC

A series of runs was carried out on problems of the general form shown in Fig 2. For these calculations an array of 91 cylindrical cells was set up on a hexagonal lattice within an otherwise unoccupied cylindrical region representing the blanket. The cells were defined as SPECIFIC rod regions (Appendix B) and consisted of liquid lithium contained in niobium cladding equivalent to 6% of the cell volume. Blanket depths of 50 cm and 100 cm were considered, with a distance between adjacent cell centres of either 60 cm or 120 cm. The end walls of the cells were not represented. Above the cells is a reflector of iron 100 cm thick, followed by the upper reflecting boundary to the problem space.

In order to simulate tapered gaps several runs were performed with cells of smaller radius, but with the same 60 cm or 120 cm pitch spacing corresponding to various values of the visibility parameter VIS in Fig 3. Results are detailed in Table I. The main aim of the calculations was to provide information on the net neutron current leaking into the reflector. This was monitored by integrating the cross sections for neutron absorbing reactions in iron over the reflector spectrum.

To isolate the effect of the inhomogeneity of the cellular blanket from the density reduction effect further computations were carried out in which the 91 cell array and the gaps between cells were homogenised. Two models were used: (i) a homogeneous blanket of Li + 6% structure to the full physical density and with no voids, corresponding to an "onion skin" blanket of the same depth, and (ii) a low density homogeneous blanket corresponding to cells packed to a diameter/pitch ratio, $\alpha = 0.90$.

While neutron leakage to the reflector is an important factor in a fusion reactor design, an equally pertinent one is the tritium breeding ratio. However, using a Monte Carlo method in which the results are always subject to statistical errors, it is much better to investigate the reflector current, which undergoes a much greater relative change than the breeding ratio as a result of introducing the cellular blanket. The impairment of breeding performance can be obtained from the increase in net reflector current by comparison with previous "onion skin" model calculations, as discussed in Section 9.

5. RESULTS

In the SPECIFIC runs, the integration routine was used to obtain the reaction rates over the whole reflector for the neutron absorbing reactions in iron. Referring to Fig 2 and the dimensions thereon, this gives an estimate of the total net current of neutrons leaving the upper surface of the blanket over a circle of radius 291.54 cm, the across flats dimension of the 91 cell array, over which neutrons are permitted access to the reflector. This current has been increased by a factor to take into account radial fall-off over the width of the array. The factor ϕ central/ϕ mean has been calculated from the radial distribution of total neutron flux in a very thin layer of iron immediately above the cell array. The corrected current J appears in column 5 of Table I. Errors quoted are those calculated by the SPECIFIC code from the variance in the computed fluxes. SPECIFIC breaks down the total number of source neutrons dealt with into smaller sub-units or "experiments", each of which yields an estimate of the flux in any region of interest, from which the mean and variance are obtained for the total number of neutrons tracked.

The net neutron current to the reflector when the blanket is homogenised appears as J_{homog} in column 6 of Table I. It is obtained by interpolation for homogeneous cases other than those calculated.

TABLE I

Neutron Currents Penetrating Lithium/Niobium Blankets

1. Case No	2. Blanket Thickness cm	3. Pitch, cm	4. $\alpha = \frac{\text{Rod Diam.}}{\text{Pitch}}$	5. J = net leakage current	6. J_{homog}	7. J/J_{homog}	8. VIS	9. VIS $\{\text{cell radius}\}^2$
RAD 35	50	homogeneous at full physical density		651 ± 40	-	1	0	0
37	50	homogeneous at density equivalent to α = 0.90		851 ± 42	-	1	0	0
34	50	120	1.00	836 ± 46	723	1.156	4.83	17.4×10^3
36	50	120	0.95	882 ± 47	792	1.114	28.54	102.7×10^3
38	50	120	0.93	1015 ± 50	818	1.241	46.5	167.4×10^3
42	50	60	1.00	647 ± 40	723	0.894	4.83	4.3×10^3
44	50	60	0.90	804 ± 45	851	0.944	84.1	75.6×10^3
80*	50	120	0.95	889 ± 47	792	not used in fitting results		
RUD 35	100	homogeneous at full physical density		217 ± 26	-	1	0	0
37	100	homogeneous at density equivalent to α = 0.90		416 ± 33	-	1	0	0
34	100	120	1.00	322 ± 28	269	1.197	4.83	17.4×10^3
40	100	120	0.90	562 ± 37	416	1.350	84.1	302.0×10^3
44	100	60	0.90	399 ± 32	416	0.960	84.1	75.6×10^3

* RAD 80 is a special case discussed in Section 8. It differs from case No RAD 36 in that the lithium and niobium are homogenised, the gaps between the cells meanwhile retaining the same geometry

The ratio J/J_{homog} is also tabulated. Column 8 gives the value of VIS, while in column 9 the product VIS.(cell radius)^2 is given.

6. ANALYSIS OF THE RESULTS

In the SPECIFIC output the fluxes quoted are normalised to a total source of 10^4 neutrons. Since in the process of producing a representative angular distribution of incident 14 MeV neutrons on the first wall, many of the neutrons emitted from the cylindrical source region are wastefully expended without entering the blanket, the currents given in Table I do not give a true measure of the neutron loss. Appendix G gives details of the method of normalising the results by relating the neutron current leaking into the reflector to the 14 MeV neutron current incident normal to the first wall. This has been done for a particular reactor model in which the first wall radius is 600 cm, with a plasma radius of 480 cm. The total net neutron current leaking from the blanket into the reflector, expressed as a fraction of the total neutron source, is given by:

2.71×10^{-4} J for 50 cm blanket depth (i)

and 2.92×10^{-4} J for 100 cm blanket depth (ii)

In analysing the results of Table I for various blanket configurations, it is proposed that the neutron current leakage into the reflector can be expressed as that leaking from a homogeneous blanket of the same mean density, increased by an inhomogeneity factor F, dependent on the gap geometry. The form of this dependence, it can be argued, is a proportionality to both VIS and the square of the radius of the cells. The latter factor arises from geometrical consideration of the solid angle subtended at the rear end of the gap between cells by the area of the gap at the first wall end visible to it. On this basis the inhomogeneity factor J/J_{homog} has been plotted against VIS (cell radius)^2 in Figs 5 and 6 for 50 cm and 100 cm deep blankets respectively. Straight lines

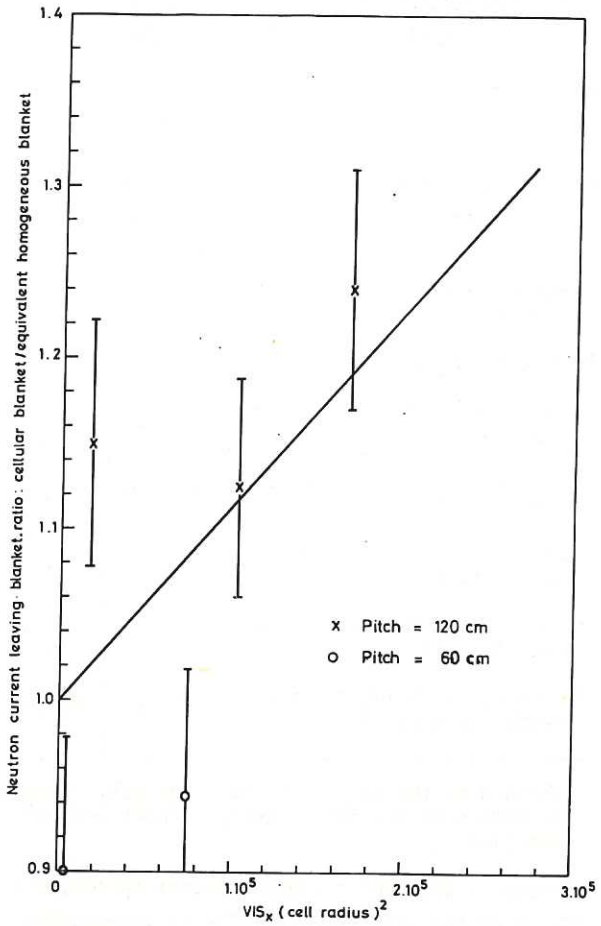

Fig.5 Inhomogeneity effect in 50cm thick blankets.

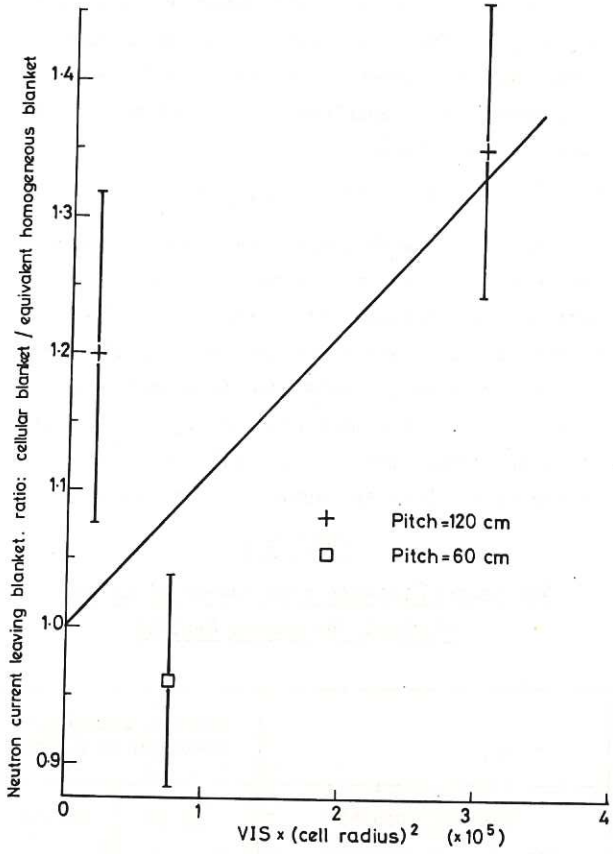

Fig.6 Inhomogeneity effect in 100cm thick blankets.

fitted by least squares analysis give the following expressions for the inhomogeneity factor F:

$$F_{(50)} = 1 + 1.14 \times 10^{-9} \times \text{VIS.(radius)}^2 \quad \text{for 50 cm blankets} \qquad \text{(iii)}$$

$$F_{(100)} = 1 + 1.09 \times 10^{-9} \times \text{VIS.(radius)}^2 \quad \text{for 100 cm blankets} \qquad \text{(iv)}$$

7. PREDICTED PERFORMANCE OF PRACTICAL BLANKETS

(a) Blankets with parallel cells

Using the above expressions (i) and (ii) for the normalised neutron leakage from the blanket, together with the inhomogeneity factor (iii) and (iv), the effects of close-packed cellular configurations with parallel cells can be predicted as in Table II below.

The increase in neutron leakage of 2.4% from the full density blanket to that in which cells of 60 cm radius and 50 cm depth are arranged in a hexagonal lattice compares well with the estimate of Appendix A in which duct transmission of 0.93% of the 14 MeV neutrons and 1.15% due to neutrons reflected from the first wall opposite combined to give a net loss of 2.15%. The agreement is considered to be fortuitous, however, since

TABLE II

Net Neutron Leakage from Close-Packed Cellular Blankets Per Source Neutron

	Neutron Leakage as Fraction of Source	
Blanket "depth"	50 cm	100 cm
Full density blanket	0.176	0.063
Homogenised blanket 90.7% density corresponding to cellular blanket	0.196	0.078
Cellular blanket 30 cm radius cells	0.1965	0.0784
Cellular blanket 60 cm radius cells	0.200	0.0795

Appendix A gives no consideration to reflection of neutrons into the blanket by the iron reflector. There is also inherent in Appendix A the unwarranted assumption that the 14 MeV neutron flux falling on the gap at the first wall is isotropic and, further, no account is taken of enhanced penetration by neutrons following paths which cross both lithium

blanket material and gaps. This result would be applicable to the plane parts of the torus for a "lobster back" model blanket. The very modest increase in leakage does not, however, take into account the effects of neutron leakage at the intersections between the planes of cells where much more severe departures from the homogeneous ideal can be expected.

(b) Non-parallel Cells of Uniform Size

When cells with tapered gaps between them are considered, the visibility parameter VIS (see section 3 and Appendix F) is increased. The effective taper, and hence the value of VIS, varies around the minor circumference in a manner discussed in Appendix H. The mean neutron leakage over the cellular blanket for various cell radii and depths is evaluated there and summarised in Table III.

TABLE III

Net Neutron Leakage from Non-parallel Cell Blanket, Per Source Neutron

	Neutron Leakage - Fraction of Source	
Blanket "depth"	50 cm	100 cm
Full density blanket	0.176	0.063
Mean void fraction in blanket	13.4%	17.7%
Leakage fraction homogeneous blanket of same void fraction	0.204	0.097
Cellular blanket, cells 30 cm radius	0.208	0.100
Cellular blanket, cells 60 cm radius	0.219	0.109

(c) Non-parallel Cells of Varying Size

A point neglected in deriving the values in Table III is that mentioned already in section 3(c), viz that it is impossible to achieve a close-packed hexagonal array of cells of uniform size on a toroidal surface. In Appendix H the arguments are further extended to the case of a hexagonal array of touching cells on the toroidal surface, whose radii increase around the minor circumference from the hub to the tread side, considering the torus as a tyre. The resulting mean neutron leakage from the blanket is as shown in Table IV.

TABLE IV

Net Neutron Leakage Fraction from Non-parallel Cells of Position Dependent Radius

	Neutron Leakage - Fraction of source	
Blanket "depth"	50 cm	100 cm
Leakage fraction full density blanket	0.176	0.063
Mean void fraction in blanket	13.4%	17.7%
Leakage fraction, homogeneous blanket	0.204	0.097
Range of cell radius, hub to tread 30 - 60.5 cm	0.214	0.106
* Increase in blanket depth needed to compensate	10 cm	29 cm
Range of cell radius, hub to tread 45 - 91 cm	0.226	0.116
* Increase in blanket depth needed to compensate	13 cm	36 cm

* Defined as the additional depth of cells needed to return to the full density blanket leakage fraction.

8. FLUX INHOMOGENEITY IN THE REFLECTOR DUE TO THE CELLULAR BLANKET

From the standpoint of engineering of the reflector shield and cryogenic magnet system, the effects of the gaps between cells in introducing local hotspots are of crucial importance. A further case (RAD 80) was run to investigate the flux variations in the reflector. RAD 80 differed from its nearest equivalent, RAD 35, (see Table I) in that the lithium and niobium cladding in each cell were homogenised to economise on computer storage. Immediately above the 91 blanket cells was a very thin iron layer containing iron discs (rods in the SPECIFIC connotation). The discs were of the same radius and on the same centres as the blanket cells. The remainder of the 100 cm thick iron reflector lay above that. SPECIFIC gave the fluxes in the discs and in the iron between the discs separately, the latter corresponding to the outer end of the gaps in the blanket. The ratio mean fluxes "behind" the gap to mean flux behind the blanket cells was 2.40 ± 0.2 for 14 MeV neutrons and did not differ significantly from this value at other energies, suggesting that a large part of the streaming down the gaps is of low-energy neutrons emitted by the opposite first wall. This gives an upper limit in this case for the inhomogeneity of the fluxes and therefore local heating and damage rates in the reflector. Considerable smoothing out can be expected for greater penetration into the reflector and shield as a consequence of neutron scattering and geometrical

factors.

9. IMPAIRMENT OF TRITIUM BREEDING

A factor of considerable interest to the fusion reactor designer is the tritium breeding ratio. Table V shows the breeding ratios from both the $Li^6(n,\alpha T)$ and the $Li^7(n,n'\alpha T)$ reactions as well as the neutron leakage fraction for idealised full density "onion skin" blankets of 50 cm and 100 cm depth. Clearly there is a link between these parameters. Neutrons leaking from the blanket are no longer available to it for tritium breeding. On increasing the blanket depth the fall in leakage fraction from 0.245 to .078, i.e. 0.167, led to an over-all breeding ratio increase of 0.23. A one to one correspondence between neutron loss and breeding loss is not observed since some of the neutrons leaving the blanket are of high energy and could have taken part in the $Li^7(n,n'\alpha T)$ reaction which breeds tritium and leaves a secondary neutron still able to breed via the $Li^6(n\alpha T)$ reaction. Since the spectrum shape as calculated at the outer end of the gaps in the blanket is similar to that behind the cells it is reasonable to assume that the neutrons lost through the gaps and by the density reduction effect are responsible for a breeding loss in the same proportion. The breeding loss is therefore .230/.167 = 1.38 times the increase in neutron leakage from the blanket.

TABLE V

Neutron Leakage Fraction and Tritium Breeding, T, in Infinite Cylinder "onion skin" Model Blankets

Case No	Blanket Thickness cm	Neutron Leakage Fraction	T_6	T_7	T
OIL A	50	0.245 .008	.73	.64	1.38
OIL B	100	0.078 .002	.86	.75	1.61

10. CONCLUSIONS

Calculations carried out on blankets comprising lithium filled niobium cells of practical dimensions have shown that the extra neutron losses incurred as a result of discarding the original "onion skin" concept for a cellular design are not disastrously large. It is clear that for all reasonable cell radii the effect is mainly due to the reduction in blanket mean density. It has been shown that for a model with cells of radius ranging from 30 cm at the hub side of the torus to 60.5 cm at the tread the increase in neutron loss is only 1/3 greater than that resulting from the exercise of reducing a homogeneous "onion skin" blanket to the same mean density as the cellular one. This leads to a fall in the tritium breeding ratio which can be compensated by an increase in depth of the cell. On this basis for blankets 50 and 100 cm deep with void fractions of 13.4% and 17.7% the compensating depth increases would have to be about 10 cm and 29 cm respectively. These are considerable increases, especially in the case of the 100 cm blanket, which might be necessary if flibe were to be used as a breeding material. Fortunately, however, it has always been recognised that blankets would be prone to loss of breeding performance by virtue of inhomogeneity introduced by injectors, divertors, etc, as well as the gaps between cells, and reference reactor designs have always been prepared with some allowance for this in hand. These allowances, amounting to 15% (i.e. T = 1.15) in UKAEA designs, are adequate for the examples above, which, for their nominal depths of 50 cm and 100 cm would have tritium breeding shortfalls of 5.2% and 5.9% respectively.

A further consequence of blanket inhomogeneity will be "hotspots" in the reflector and, to a lesser extent, in the magnet shield. A typical case quoted in section 8 shows a peak to mean ratio of flux and, by inference, heat deposition rate of 2.4 across the reflector material immediately behind the blanket. Further calculations will be necessary to explore the way in which this is smoothed out as a function of depth into the reflector and magnet shield and determine the additional depth of shield required to keep the nuclear heating in the superconducting coils at an acceptable level.

11. ACKNOWLEDGEMENTS

The authors would like to record their grateful thanks to Mr J T D Mitchell and Mr M W George for many stimulating and helpful discussions on fusion reactor technology.

12. REFERENCES

(1) Dänner, W. Neutron flux asymmetry in toroidal geometries. IPP 4/101, (1972).

(2) Mitchell, J T D and Booth, J A. Wall loading limitations in a helium cooled fusion reactor blanket, CLM R126, (1973).

(3) George, M W. Structure renewal and maintenance requirements in a fusion reactor, 5th Symposium on Engineering Problems of Fusion Research, Princeton, November, 1973.

(4) Stanbridge, J R et al. Design of stainless steel blanket cells for a fusion reactor, CLM R127, (1974).

(5) Ruffle, M P. SPECIFIC. A Monte Carlo program for high energy neutron spectrum estimation, AERE R4553.

APPENDIX A

Neutron Transmission between Cylindrical Blanket Cells. Approximate Calculation

Consider a nest of cylindrical cells comprising a toroidal fusion reactor blanket[2], which touch each other along adjacent sides as in Fig. 1., leaving a three cornered cusp shaped gap between them whose axis points towards the minor axis of the plasma. At point A, at the centre of the cusp on the outside of the blanket a part of the volume of the plasma is in view through the gap. This volume is bounded by a tapering cusp-shaped surface. If the cells are of radius r and depth h then the cusp shaped triangle at the first wall end of the gap, which has an area $0.161\ r^2$, subtends a solid angle of approximately $0.161\ r^2/h^2$ at A. If the plasma emits neutrons isotropically at S n cm^{-3} s^{-1} it can be shown that the flux at A arriving from the plasma volume intersected by this solid angle is given by

$$\phi = \frac{0.161\ r^2}{h_2} \cdot \frac{S}{4\pi} \cdot 2a$$

where 2a is the minor diameter of the plasma, ie the depth of plasma as seen from A. This is approximate, becoming in error if the tapered volume subtends too wide an angle, in which case the depth of plasma viewed is not constant.

In practical terms this flux is equivalent to a current since the neutrons have been collimated to a large extent. Since the cusps occupy a fraction $0.161/\sqrt{3} = 0.0931$ of the area of the outside face of the blanket, and assuming that point A is typical of the whole of the cusp's area, the neutron leakage current by transmission through the gaps averaged over the outer blanket surface is:-

$$\bar{J} = \frac{0.161\ r^2\ S\ a\ .\ 0.0931}{2\pi h^2} \qquad (v)$$

The neutron output of the plasma is $\pi a^2 S$ per unit length and in the absence of a blanket the mean leakage current at R', the blanket outer radius, would be $\pi a^2 S/2\pi R'$. The fraction of the neutron output lost by direct shine along the gaps is thus

$$\frac{0.161\ r^2\ S\ a\ .\ 0.0931\ .\ 2\pi R'}{2\pi h^2 \qquad \pi\ a^2\ S} = 0.00477\ \frac{r^2 R'}{h^2 a} \qquad (vi)$$

Let us insert typical values, h = 50 cm and a plasma filling 80% of the torus minor radius, giving a = 480 and R' = 650 cm. Then for cell radius/depth ratios r/h = 15/50, 30/50 and 60/50 the neutron losses are 0.058, 0.23 and 0.93% respectively.

So far we have examined the loss of 14 MeV neutrons from the plasma. In addition neutrons reflected from the front wall opposite stand a chance of being transmitted down the gaps. The flux at the front wall, excluding the 14 MeV uncollided flux is $\sim \frac{1.04\pi n^2 S}{\rho}$ n $cm^{-2}s^{-1}$, typical of a lithium blanket with a niobium first wall. The area of the opposite wall visible at A is $0.161\ \frac{r^2}{h^2} \cdot (2\rho + h)^2$, and assuming that the flux there is isotropic, the current from that area reaching A, will be

$$J = 0.161\ \frac{r^2}{h_2}\ (2\rho + h)^2 . \frac{1.04\ \pi a^2 S}{\rho} . \frac{1}{4\pi\ (2\rho + h)^2} \qquad (vii)$$

which expressed as a mean current over the rear surface of the blanket, and compared with the plasma neutron output current at that point as before, gives leakage rates of .076, 0.30 and 1.22% for r/h = 15/50, 30/50 and 60/50 respectively.

These calculated neutron losses are surprisingly modest, and in addition do not take into account the effect of the reflector behind the cells in returning some of these neutrons to the blanket. However no account has been taken of enhanced penetration of the blanket by neutrons which pass partway through the blanket and then enter the gap or alternatively those which travel partway down the gap before entering the blanket material.

APPENDIX B

The Monte Carlo Code SPECIFIC II

SPECIFIC II is a Monte Carlo code written in IBM System/360 Fortran IV for estimating the high energy neutron spectrum from either a fission source or monoenergetic source in cylindrical (R,Z) geometry. It is described fully elsewhere[5] but the geometrical arrangements possible are briefly described here.

The problems that can be dealt with comprise basically a volume enclosed in a rectangular box, square in plan with height and square dimensions specified by the user. Neutrons can be tracked in their travels through the materials in the box by the programme and data must be supplied to instruct the programme in the eventuality of neutrons colliding with the walls of the box:- eg whether they are to be absorbed either partially or completely, or alternatively reflected. Within the box, regions can be specified bounded by horizontal plane surfaces and cylinders concentric with the vertical centre line of the box. The materials of which each of these cylindrical or annular regions is comprised must be specified and a neutron source strength can be ascribed to any of them. The

programme obtains scattering, absorption and other neutronic data it requires for the specified materials (generally a mixture of elements in proportions as given by the user) from a comprehensive library tape.

A further facility in the programme and one that is essential for our use is the ability to specify rods in any of the problem regions. These rods were included originally to simulate fuel rods in fission reactor lattice calculations. A rod consists of a cylindrical arrangement of concentric shells (to simulate cladding as well as the fuel) which fits wholly within a region of the whole problem volume. The coordinates of the axis of each rod must be specified as also must the radii of the cladding and contents as well as the materials of which they are made.

Once the programme has assembled and digested the input data, it starts neutrons from the source region in a random manner with regard to origin within the source volume and initial direction. It keeps a score of track length of neutrons crossing regions as specified by the user while within specified energy bands. The scoring regions which can include the rod regions, need not necessarily coincide with the material regions. After the tracking is completed the scores can be printed out in a choice of formats and integration of various chosen cross-sections over the neutron energy spectrum in each of the scoring regions can be undertaken.

APPENDIX C

Angular Distribution of Neutrons arriving at the First Wall

In toroidal geometry the angular distribution about the normal to the first wall with which the neutrons arrive from the plasma is a function of position around the minor circumference. The derivation of this angular distribution has been carried out by integration at 3 points, viz at the tread A, at the sidewall B, and at the hub side of the torus C in Fig 7(a). It is discussed in this Appendix for the sidewall position B, on the top of the torus. Fig 7(a) represents part of the torus and the plasma inside it. BD represents the tangent to the minor circumference at B. In order to obtain the angular distribution with respect to the normal double integration is performed numerically. The basic step in this is to select a vertical plane through B at an angle φ to the minor section of the torus. This cuts the torus and the plasma in the dotted curves as shown. The actual shapes are

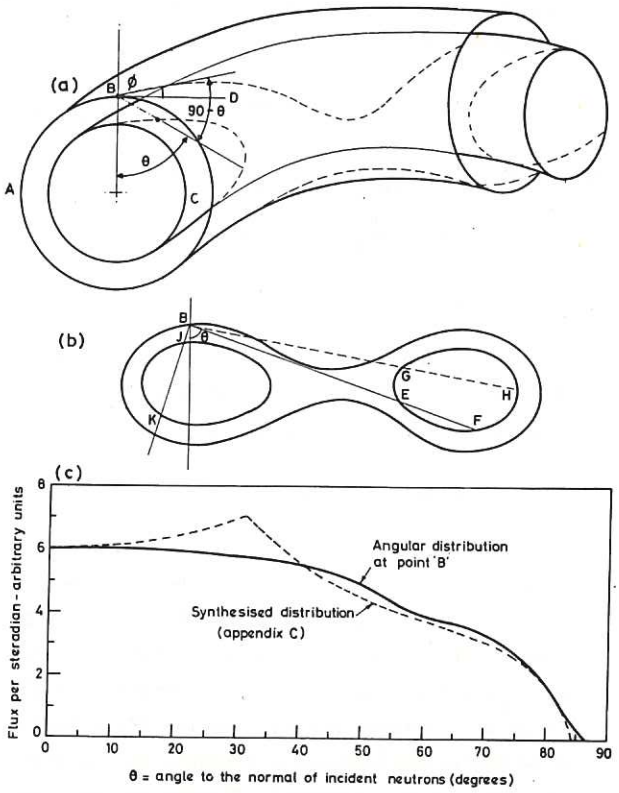

Fig.7 Angular distribution of neutrons arriving at the first wall.

only 2-dimensional since they lie in the vertical plane. Fig 7(b) shows such a section. Within the plane the shapes are given by easily derived 4th power expressions. A vector drawn at an angle θ to the normal as in Fig 7(b) cuts the torus section in either two or four roots, while it cuts the plasma section in zero, two or four roots. Logical switching is used to determine which parts of the plasma are to be included in the integration. For instance the chords EF and JK are valid parts while GH is not since a direct line of sight to B passes through the torus wall. The contribution of neutrons emitted by the element of plasma volume along the chord EF is therefore added into the computer storage bin appropriate to the angle θ, and the integration with respect to θ carried on by incrementing θ by a small amount and repeating the logical decisions governing the line of sight criteria. The resulting distribution for a torus with major and minor radii 17.8 m and 6 m respectively and a plasma radius 80% of the minor radius is shown by the solid curve in Fig 7(c).

Without carrying out extensive modifications to SPECIFIC, it is not possible to produce an anisotropic angular source distribution. The shape of the required distribution can be simulated fairly closely however, by the arrival directions at B of neutrons emitted isotropically by a thick disc as shown in Fig 2. It can be shown that a disc of radius R and thickness b situated a distance a below point B will produce

an angular flux distribution $\phi(\theta)$ about the normal given by

$$\phi(\theta) = \frac{b}{4\pi \cos\theta} \quad \text{in the range } 0 < \theta < \tan^{-1}\frac{R}{a+b}$$

and $$\phi(\theta) = \frac{1}{4\pi}\left(\frac{R}{\sin\theta} - \frac{a}{\cos\theta}\right) \text{ in the range}$$

$$\tan^{-1}\frac{R}{a+b} < \theta < \tan^{-1}\frac{R}{a}$$

and $\phi(\theta) = 0$ for $\theta > \tan^{-1}\frac{R}{a}$

By fitting a and b relative to R the required distribution can be approximated well, as shown by the dotted curve in Fig 7(c).

APPENDIX D

The SPECIFIC Model

The model shown in Fig 2 has been chosen to represent part of the blanket, embracing a large enough number of cylindrical cells (91) to obtain representative conditions over a central region. Appendix C explains how the angular distribution of 14 MeV primary neutrons incident on the first wall has been represented. Towards the edge of the 91 cell array the angular distribution of arriving neutrons will depart from that produced at the centre by the cylindrical source. In particular while it will be accurate for neutrons arriving normally to the first wall, the neutron current per steradian arriving at an angle to the normal will fall short of that required towards the edge of the array, though there will be some numerical compensation in that extra neutrons will arrive at larger angles than the cut-off angle in Fig 7(c). These shortcomings are not serious over most of the cell array. Having simulated the source angular distribution adequately over most of the cell array, the next step is to ensure that the spectrum of lower energy neutrons at the underside of the blanket, ie at the first wall, is representative. To achieve this all the neutrons leaving it must be reflected back into it with the same angular distribution and energy spectrum. A horizontal reflecting plane is specified as the lower problem boundary. This reflects at the same angle neutrons leaving the first wall close to the normal direction which would be the most penetrating when falling on gaps in the first wall at the opposite side of the minor diameter of the torus. To conserve all the neutrons leaving the first wall of the 91 cell blanket array the sides of the square box defining the problem space are also made reflecting. This in turn introduces problems with the source specification since side reflections would bring neutrons from unwanted directions. This was solved by writing into the data library a medium code named FAB (Fast Absorber) which has the property of absorbing 14 MeV neutrons while being transparent to all others. By placing this around the radial boundaries of the source cylinder unwanted 14 MeV neutrons are absorbed.

The source volume was specified with a radius equal to the across flats dimension of the 91 cell array. This prevented neutrons from the source streaming up the gap as at point B in Fig 2 and entering the sides of the outermost cells. The region encircling the blanket is composed of an neutrons leaking sideways from the multi-rod region representing the blanket cells and any neutrons coming directly from the source region and thereby prevents by-passing of the blanket. Below this ABS region lies another region similar in plan but very thin, consisting of SCAT, a material that has a very high scattering cross-section but with zero absorption at all neutron energies. This serves the purpose of reflecting low energy neutrons back into the region below the blanket, thus keeping the first wall spectrum representative. A further ring of ABS was placed over the multi-rod region with an inner diameter equal to the across flats dimension of the 91 cell array, thus sealing off access of neutrons to the reflector other than through the blanket cells or representative gaps between the cells. The upper part of Fig 2 shows the disposition of these regions, the lower part of Fig 2 showing an isometric diagram of the source volume and part of the 91 cell array.

The performance of a particular arrangement of the blanket cells in breeding tritium could not be judged directly since radial leakage from the 91 cell array could not be accounted for accurately. In any case as discussed in section 4 of the main text a more sensitive parameter is the neutron current leakage from the top of the blanket cell array into the reflector. By integrating the neutron absorbing reactions $(n\alpha)$, (np), $(n\gamma)$ and $-(n2n)$ over the neutron spectra within the iron reflector the net number of neutrons leaving the lithium blanket was obtained. The negative sign applied to the (n2n) reaction is indicative of the fact that it produces neutrons which increases the lower energy flux and enhance the $n\gamma$ capture rate.

APPENDIX E

Volume of Voids in Blankets Composed of Cylindrical Cells

Cells Around a Straight Pipe

The simple case of prismatic blanket cells of depth h clothing a straight pipe of radius r as in Fig 8 will be dealt with first. If the cells are

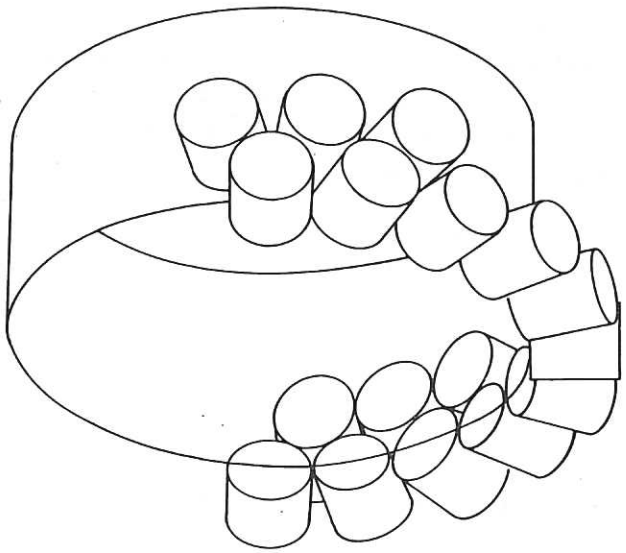

Fig.8 Cylindrical cells fitted around a straight cylinder.

hexagonal with their ends close nested and touching the pipe then their volume is equal to the product of the pipe's surface area and the blanket depth ie 2π rh per unit length of pipe. Since the blanket volume is $\pi (r+h)^2 - \pi r^2 = \pi(2rh+h^2)$ the void fraction is given by $\pi h^2/\pi (2rh+h^2) = h/(2r+h)$. If the cells are touching cylinders instead of hexagonal prisms, their ends cover 90.69% of the pipe surface and the void fraction then becomes

$$V.F. = \frac{\pi h^2 + 2\pi rh(1-.9069}{\pi(2rh+h^2)} = \frac{h + 0.1862\ r}{(2r+h)} \qquad \text{(viii)}$$

Cells Around a Torus

When cylindrical cells are positioned end-on against a toroidal surface, two complications ensue. Firstly, in order for each to maintain side contact with 6 neighbours the radius of the cells must vary around the minor circumference. It is assumed that in this distorted hexagonal lattice the figure of 90.69% for the area coverage still holds. Secondly, side contact between cells occurs at the toroidal surface only between the tread and the sidewall. From the sidewall to the hub the opposite curvatures of the toroidal surface lead to side contact being made at their outer ends between horizontally adjacent cells and at their first wall ends for neighbours around the torus minor periphery as in Fig 4.

For the region between the sidewall and the tread ($\pi/2 < \omega < \pi$ in Fig 4) the toroidal surface has positive curvatures in both minor and major circumferential directions. These are respectively $\frac{1}{\rho}$ and $-\cos\omega/(R-\rho\cos\omega)$. Adding these we obtain the combined surface curvature $C = (R-2\rho\cos\omega)/(R-\rho\cos\omega)$ and the ω dependent void fraction may be derived by substituting $\frac{1}{C}$ for r in the case of cylinders covering a straight pipe in equation (viii). Over the range $\frac{\pi}{2} < \omega < \pi$ the cylindrical cells occupy a volume given by the product of their depths and 0.9069 times the surface area of the toroid from sidewall to tread, viz.

$$.9069 \int_{\frac{\pi}{2}}^{\pi} 2\pi(R-\rho\cos\omega)\,\rho d\omega = 5.70\ h\ (\tfrac{\pi}{2} R\rho + \rho^2) \qquad \text{(ix)}$$

In the range $o < \omega < \frac{\pi}{2}$ the cells touch their horizontal neighbours at the outer ends as in Fig 4 and a gap develops at their first wall end such that the ratio of diameter to pitch (1.0 at the outer end) becomes $(R-(\rho+h)\cos\omega)/(R-\rho\cos\omega)$. Instead of a fraction .9069 of the torus surface being covered by cell ends, it is reduced by this diameter to pitch ratio (a function of ω). Over the range $o < \omega < \frac{\pi}{2}$ the cells occupy a volume

$$h \times 0.9060 \times \int_0^{\frac{\pi}{2}} 2\pi\ \frac{(R-\rho\cos\omega)(R-(\rho+h)\cos\omega)}{(R-\rho\cos\omega)}\,\rho d\omega \qquad \text{(x)}$$

$$= 5.70\ h(\tfrac{\pi}{2} R\rho - \rho^2 - \rho h) \qquad \text{(xi)}$$

Combining (ix) and (xi) the total volume of blanket cells over the range $o < \omega < \pi$ is $V_{cells} = 5.70h\ (\pi R\rho - \rho h)$ while that of the blanket space over the same range is $V_{blanket} = \pi^2 R(\rho+h)^2 - \pi^2 R\rho^2 = \pi^2 R(2\rho h+h^2)$. Numerical values of the void fraction for different blanket depths are given in Table III.

Improved Packing of Cells on the "Inside" of the Torus

In the context of a hexagonal packing of blanket cells rather than the square array of Fig 4 the above assessment is pessimistic over the range $o < \omega < \frac{\pi}{2}$ since the gaps between horizontally adjacent cells at their first wall ends afford the opportunity to bring the neighbours in the minor circumference or "vertical" direction closer as in Fig 9(a). Alternatively if the "hexagonal" array of cells is orientated as in 9(b) then the gaps between outer ends of adjacent cells around the minor periphery give opportunity for closing up or "nestling" the horizontally adjacent cells. It is clear that the angle between "vertically" adjacent cells is greater in Fig 9(b) than that between horizontally adjacent cells in Fig 9(a) provided $\rho < R - \rho - h$. The arrangement represented by Fig 9(b) offers more scope for nestling of the horizontal neighbours and thus will achieve a higher packing of cells into the blanket zone. The packing fraction of cells in the blanket volume is

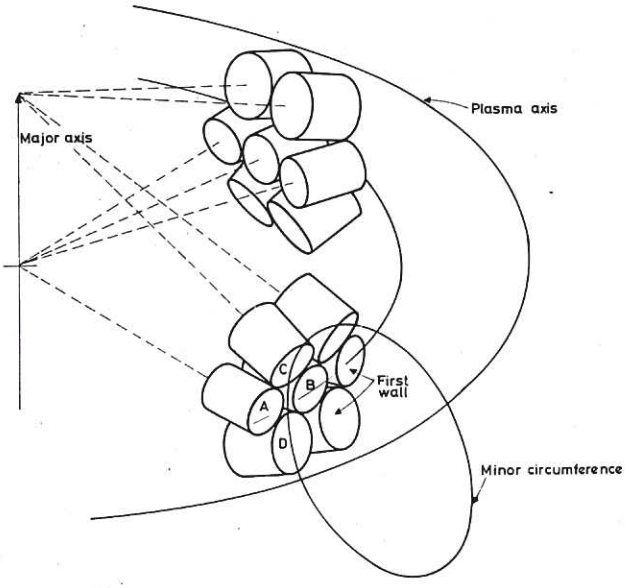

Fig.9(a) Cells on a toroidal surface.

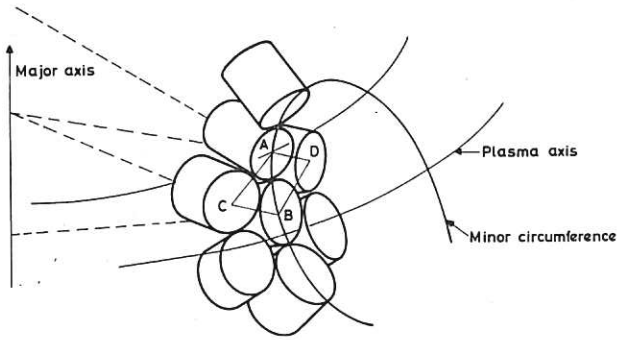

Fig.9(b) Cells on a toroidal surface (alternative orientation).

influenced by the ratio of the area of the cell end to that of the lattice area ABCD, in which the separation CD plays a crucial part. Consider the plan view in Fig 9(c) in which O represents the

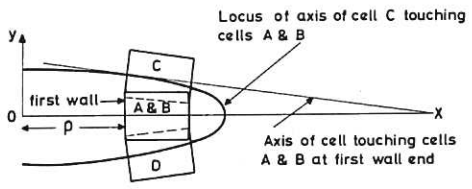

Fig.9(c) Plan view of adjacent cells.

intersection of the axes of cells A and B with the plasma axis. Cells A and B are superimposed on the plan. The axis of cell C which touches both A and B is a tangent to an ellipse centred at O with minor and major axes equal to D, the cell diameter and 2ρ respectively, whose equation is

$$\frac{x^2}{(2\rho)^2} + \frac{Y^2}{D^2} = 1 \text{ which when differentiated gives} \qquad \text{(xii)}$$

$$\frac{dy}{dx} = -\frac{D^2}{4\rho^2 y} \qquad \text{(xiii)}$$

The tangent to this ellipse at the front wall point P defines the axis of a cell which could be placed against cells A and B. The point X', (fig 9(c)) at which the tangent to the ellipse intersects its major axis is given by

$$X' = x - y\frac{dx}{dy}, \text{ which for } x = \rho \text{ (cells touching at the first wall)} \qquad \text{(xiv)}$$

$$\text{gives } X' = \rho + \frac{4\rho^2}{\rho} \cdot \frac{Y^2}{D^2} =$$

$$\rho + 4\rho\left(1 - \frac{\rho^2}{4\rho^2}\right) = 4\rho \qquad \text{(xv)}$$

From this it is clear that for an aspect ratio exceeding 4, cells <u>can</u> be arranged in a hexagonal configuration with each cell touching 6 neighbours at the first wall end over the whole toroidal surface. For a lower ratio the cell C will touch cells A and B either at the level of the rear wall or at some intermediate point part way down the cell. A close-nested first wall configuration can be maintained for $\omega > \phi$ where $\cos\phi = \alpha/4$ (α is the aspect ratio). Over the range $\phi > \omega > \psi$ cell C touches cells A and B at points along their length and for $\psi > \omega > o$ they touch at the rear wall. ψ is obtained by setting $x = \rho + h$, solving for X' in (xiv) and deriving ψ from the relation $\cos\psi = R/X'$. The values of ϕ and ψ are given in Table VI. The volume occupied by the cells is obtained by calculating the ω dependence of the separation of horizontally adjacent cells (CD in Fig 9(b)) and incorporating this in equations (ix) and (x). In the range $o < \omega < \psi$ cell C touches A and B at the rear wall end and the volume of cells is

$$V_o^{\psi} = .9069h \int_o^{\psi} 2\pi(R-(\rho+h)\cos\omega)\ \rho d\omega \qquad \text{(xvi)}$$

In the range $\phi < \omega < \frac{\pi}{2}$ the cells touch at the front wall (ie CD takes its minimum value) and an equation of the same form as (ix) applies:

$$V_{\phi}^{\frac{\pi}{2}} = .9069h \int_{\phi}^{\frac{\pi}{2}} 2\pi\ (R - \rho\cos\omega\ )\ \rho d\omega \qquad \text{(xvii)}$$

In the range $\psi < \omega < \phi$ the separation CD varies with the point of contact of cell C with cells A and B. The "$(\rho+h)$" term in the integrand in equation (xvi) must be replaced by x the distance of this point of contact from the plasma axis, given by

$$x = \frac{4\rho}{X'} = 4\rho^2\ \frac{\cos\omega}{R} \qquad \text{(xviii)}$$

whereupon the volume occupied by cells in this range becomes

$$V_{\psi}^{\phi} = .9069h \int_{\psi}^{\phi} 2\pi\ \left(R - \frac{4\rho^2\cos^2\omega}{R}\right)\ \rho d\omega \qquad \text{(xix)}$$

The contributions from the several ranges of ω in (ix), (xvi), (xvii) and (xix) are added to obtain the total cell volume in the torus. Table VI gives the voidage associated with each configuration of cellular blanket

Table VI Voidage in Cellular Blankets

	Voidage Fraction	
Blanket Depth	50 cm	100 cm
Cellular Blanket, on plane surface	9.3%	9.3%
Cellular Blanket on cylindrical surface of radius 6 metre	12.9%	16.3%
Cellular Blanket on toroidal surface, major and minor radii 17.8 m and 6 m	13.7%	17.8%
Cellular Blanket on toroidal surface with "improved packing" or nestling as in Fig 9(b)	13.4%	17.7%
Angular range over which cells touch horizontal neighbours at first wall end $\omega >$	42.1^{o}	42.1^{o}
Angular range over which cells touch horizontal neighbours at rear wall end $\omega <$	36.5^{o}	30.1^{o}

APPENDIX F

Calculation of Line of Sight Visibility through Tapered and Parallel Gaps

In considering the neutron leakage through gaps between cells in the fusion reactor blanket account must be taken of their complicated geometry which arises as a result of clothing a toroidal surface with parallel-sided cells. The tapered gaps cannot be modelled exactly with the SPECIFIC Monte Carlo programme, which at present can only deal with parallel arrays of cylinders. The approach adopted is to set up such a model as in Fig 10(b) whose line of sight gap leakage characteristics have been estimated to be the same as those in the practical case Fig 10(a). The line of sight leakage is calculated purely from the geometrical factors involved in the penetration of neutrons from the first wall end of the blanket to the rear. No account has been taken of attenuation effects on neutrons passing part-way through blanket material and part-way through a gap in establishing equivalent parallel and tapered configurations. It is felt that direct line of sight provides the most relevant criterion since it accounts for the most penetrating neutrons.

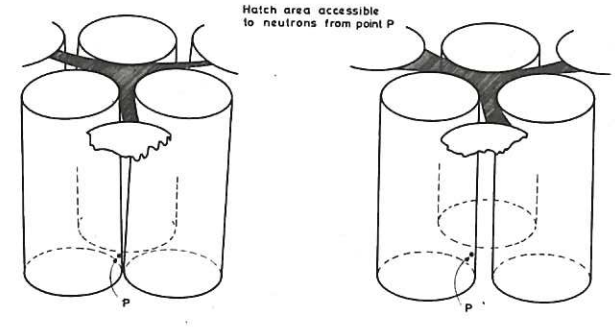

(a) Cells with tapering gaps (b) Parallel cells

Fig.10 Practical and representational arrangements of blanket cells.

In estimating the line of sight leakage through a particular gap configuration two parameters must be specified, ie the ratio of the cell diameter to the pitch between adjacent cells at the outer and first wall ends of the cells α and β respectively. The visibility or VIS is then defined as a double integral, being the integral over the gap in the first wall of the area of the rear wall gap visible to it. The assumption that the neutron leakage through a gap is proportional to the value of VIS hinges on the twin assumptions that (a) the neutron flux incident on the first wall is isotropic and (b) the solid angle subtended at a point at one end of the blanket by the gap at the other end is proportional to the area of gap visible. This will only be true if the gaps are small relative to the blanket depth.

Fig 11 illustrates the configuration of adjacent cells in plan view, as viewed along the axis of the tapered gap centred at O. The full circles represent the first wall ends of the cells while the dotted circles represent their rear wall ends. Strictly the plan view of a tilted circular disk is an ellipse but for the tapers encountered in practice the discrepancy is small. The integration is performed over the unit gap FGHJKL at the first wall end of the blanket. This is sub-divided into elemental areas $rd\theta$ by dr with co-ordinates (r,θ). One such elemental area at the point A is visible to the area ORSTUVW at the rear wall end of the blanket. The integration is not carried out on the analogous shapes along the other two legs of the gap (ie through FG and KL) since by symmetry they will be included during the integration with respect to r and θ around the point O. Points R and W on the dotted circles have co-ordinates $\theta = \pm \pi/3$ while AS and AV are tangents to the circles from A. If AX is the tangent to the full circle ie the first wall end of the cell, XV represents the line along the curved cell wall just visible by line of sight from A. By constructing VU parallel to AX we ensure that it represents a line in space lying both in the plane

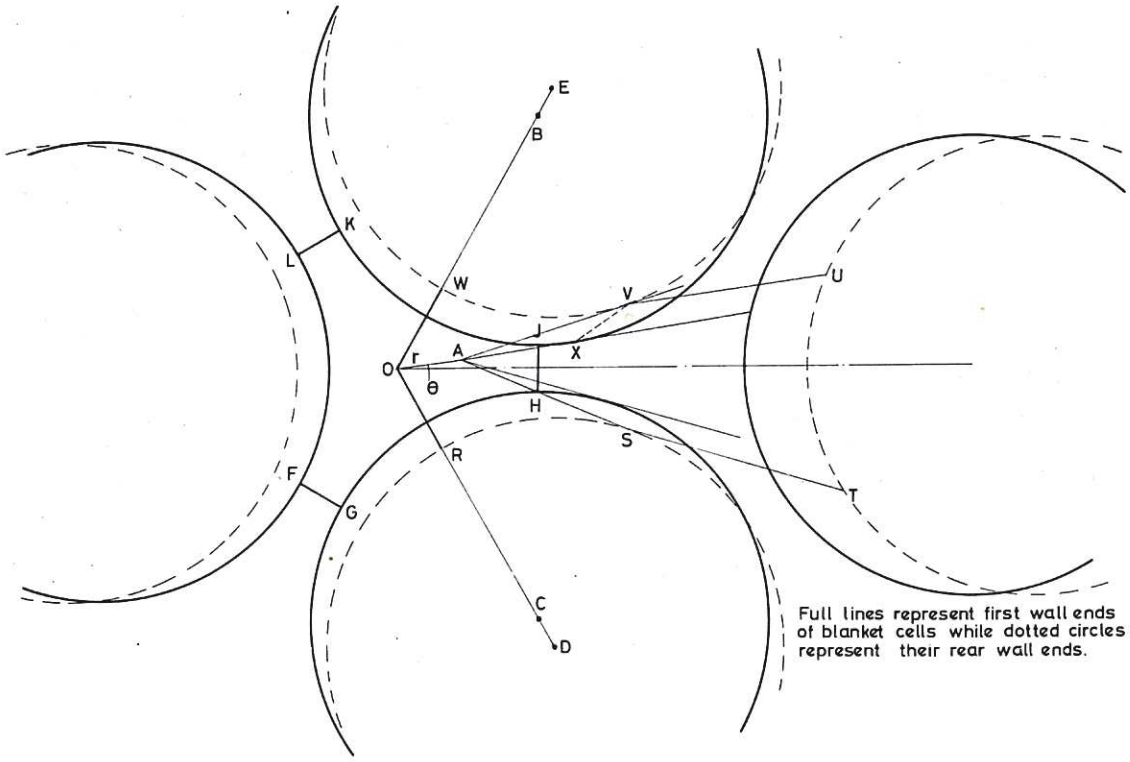

Fig.11 Plan view of a non-parallel array of blanket cells.

of the blanket rear wall and in the AXV plane. VU thus represents the limiting line of visibility from A, ST is obtained likewise. The area ORSTUVW is computed as the appropriate algebraic sum of areas of triangles and sectors. The numerical integration with respect to r and θ is carried out several times sub-dividing the dr and $d\theta$ steps and repeating until the integral converges to a specified limit.

The integrations have been performed for a range of values of α and β. The condition $\alpha = \beta$ corresponds to parallel gaps (which can be modelled by SPECIFIC), while $\beta = 1$ is appropriate to cells touching at the first wall end, diverging from each other at the rear. Fig 3 shows the results for computations embracing these two conditions. The dotted line in Fig 3 illustrates its use. An array of non-parallel cells touching at the first wall, with a cell diameter/pitch ratio $\alpha = 0.90$ at the rear wall can be simulated by (ie has the same value of VIS as) an array of parallel cells with a diameter/pitch ratio of 0.945.

APPENDIX G

Normalising the SPECIFIC Results

Because of the loss of 14 MeV neutrons inherent in the method adopted for generating the correct incident angular distribution the absorption rate of neutrons in the iron reflector does not give a true picture of their penetration of the blankets when normalised to the total source. However a normalisation is possible via the neutron current incident normally on the first wall. Referring to Fig 2 and the dimensions contained therein we note that the volume strength of the cylindrical source is given by

$$S = \frac{10^4}{223.2 \times \pi \times (291.54)^2} \text{ n cm}^{-3} \qquad \text{(xx)}$$

The depth of source viewed normally by the first wall is 223.2 x 2 (because of the reflecting boundary). The neutron current penetrating the blanket at the centre is given by $J/\pi(291.54)^2$. The current penetrating normalised to a 1 cm depth of plasma generating 1 neutron per cm^3 is thus

$$j = \frac{J}{\pi(291.54)^2} \quad \frac{223.2 \times \pi \times (291.54)^2}{10^4} \quad \frac{1}{223.2 \times 2}$$

$$= 5 \times 10^{-5} \text{ J neutrons} \qquad \text{(xxi)}$$

In a fusion reactor torus of minor radius 6m, with a plasma radius of 4.8 metres, the outer surface of the blanket is situated at 650 cm or 700 cm. from the plasma axis for 50 and 100 cm blanket depths respectively. The first wall views a normal depth of 960 cm of plasma (across its minor diameter). To make this equivalent to a view of a 1 cm depth of plasma emitting at 1 n cm^{-3} would imply a source strength of 1/960 n cm^{-3} making the total source equal to $\frac{1}{960} \pi 480^2$ for a 1 cm long section of the plasma. The total neutron loss from a 1 cm long section of the blanket is then 5×10^{-5} J x 2π x

(650 or 700), giving the neutron loss as a fraction of the production in the plasma as

$$\frac{960 \times 5 \times 10^{-5} J \times 2\pi\ (650 \text{ or } 700)}{\pi \times 480^2} = 2.71 \times 10^{-4}\ J \text{ for 50 cm blankets}$$

$$2.92 \times 10^{-4}\ J \text{ for 100 cm blankets.}$$

APPENDIX H

Enhanced Neutron Penetration in Cellular Blankets

In section 6 of the main text, the inhomogeneity factors F are derived for 50 cm and 100 cm deep blankets in terms of VIS the visibility factor for tapered gaps (see also Appendix F). The taper has two mutually perpendicular components due to the different surface curvatures of the toroid, given by $C_{min} = 1/\rho$ around the minor circumference and $C_{maj} = \frac{-\cos\omega}{R - \rho\cos\omega}$ in the major circumferential direction. Both are positive between the sidewall and tread. Adding the curvatures and dividing by two gives the curvature of the spherical surface equivalent in terms of the volume fraction occupied by the tapered gaps. The radius of this equivalent sphere is given by:

$$r = \frac{2}{C_{min} + C_{maj}} = \frac{2\rho(R - \rho\cos\omega)}{(R - 2\rho\cos\omega)} \qquad (i)$$

For gaps between cells of depth h, touching at their first wall end (the condition $\beta = 1$, see section 3 and Appendix F), the parameter α, the cell diameter/pitch ratio at the outer end, is given by:

$$\alpha = \frac{r}{r+h} \text{ or } 1 - \alpha = \frac{h}{r+h} \simeq \frac{h}{r} = \frac{h(R - 2\rho\cos\omega)}{2(R - \rho\cos\omega)} \qquad (ii)$$

(for 50 cm deep cells, R = 1780 and ρ = 600 cm, $1 - \alpha$ is approximately .04 and .05 at the sidewall and tread respectively). The lower curve in Fig 3 shows VIS as a function of α when $\beta = 1$. For α in the region 0.95 to 0.96, the curve can be approximated by the expression:

$$VIS = 4.83 + 312\ (1-\alpha) = 4.83 + \frac{156h(R - 2\rho\cos\omega)}{\rho(R - \rho\cos\omega)} \qquad (iii)$$

We can define an enhancement factor $\Delta = F - 1.0$ from the inhomogeneity factors $F_{(50)}$ and $F_{(100)}$ from equations (iii) and (iv) of section 6 in the main text. The enhancement factor per unit area is given by:

$$\Delta' = \frac{\Delta}{4\pi^2 R\rho} = \frac{1.14 \times 10^{-6}.VIS.(\text{cell radius})^2}{4\pi^2 R.\rho}$$

N.B. The coefficient 1.14×10^{-6} is appropriate to 50 cm deep cells.

Inhomogeneity Factor for Uniform Cells

Integrating this expression over the torus wall area, taking into account the dependence of VIS from (iii), we obtain the area weighted inhomogeneity factor:-

$$F = 1.0 + 2\int_0^{\pi} \Delta'.2\pi(R - \rho\cos\omega)d\omega$$

$$= 1.0 + \frac{1.14 \times 10^{-6}(\text{cell radius})^2}{\pi R} \cdot \int_0^{\pi} \{4.83(R-\rho\cos\omega) + \frac{156\,h}{\rho}(R - 2\rho\cos\omega)\}\, d\omega \qquad (xxii)$$

$$= 1.0 + 1.14 \times 10^{-6}(\text{cell radius})^2 \cdot (4.83 + 156\,h/\rho) \qquad (xxiii)$$

F is given in Table VII, with the appropriate coefficient substituted for the 100 cm deep blanket from (iv).

TABLE VII

Inhomogeneity Factor, F, for Uniform size, non parallel cells

	Inhomogeneity Factor, F	
Blanket depth cm	50	100
Cell radius 30 cm	1.018	1.030
Cell radius 60 cm	1.073	1.121

Inhomogeneity Factor for Varying Cell Size

In order to pack a pseudo regular hexagonal array of cylindrical cells on the torus surface, their radii must scale in proportion to their distance from the major axis of the torus, i.e. $R - \rho\cos\omega$. Thus, for cells of radius Y at the hub side of the torus the general ω dependence of the cell radius $y(\omega)$ is:-

$$y(\omega) = Y(R - \rho\cos\omega)/(R - \rho) \qquad (xxiv)$$

Taking this expression for the cell radius and inserting it in (xxii), where it must be included within the integral expression, we obtain the inhomogeneity factor weighted with area, cell size and VIS over the torus area:-

$$F = 1.0 + \frac{1.14 \times 10^{-6}\, Y2}{\pi R\,(R - \rho)^2}\int_0^{\pi}\{4.83(R - \rho\cos\omega)^3 + \frac{156h}{\rho}(R - 2\rho\cos\omega)(R - \rho\cos\omega)^2\}\, d\omega \qquad (xxv)$$

$$= 1.0 + \frac{1.14 \times 10^{-6}\ \gamma^2}{\pi R(R-\rho)^2}\left\{4.83\left(\pi R^3 + \frac{3}{2}\pi R\rho^2\right) + \frac{156h}{\rho}\left(\pi R^3 + \frac{5}{2}\pi R\rho^2\right)\right\} \qquad \text{(xxvi)}$$

This is evaluated below in Table VIII.

TABLE VIII

Inhomogeneity Factor F for Variable Size

	Inhomogeneity Factor, F	
Blanket depth cm	50	100
Cell radii 30 - 60.5 cm	1.052	1.088
Cell radii 45 - 91 cm	1.117	1.197

HER MAJESTY'S STATIONERY OFFICE

Government Bookshops

49 High Holborn, London WC1V 6HB
13a Castle Street, Edinburgh EH2 3AR
41 The Hayes, Cardiff CF1 1JW
Brazennose Street, Manchester M60 8AS
Wine Street, Bristol BS1 2BQ
258 Broad Street, Birmingham B1 2HE
80 Chichester Street, Belfast BT1 4JY

Government publications are also available through booksellers